NASA TECHNICAL NOTE

NASA TN D-4441

NASA TN D-4441

SIMILARITY SOLUTION FOR TURBULENT MIXING BETWEEN A JET AND A FASTER MOVING COAXIAL STREAM

by Leo F. Donovan

Lewis Research Center
Cleveland, Ohio

NATIONAL AERONAUTICS AND SPACE ADMINISTRATION • WASHINGTON, D. C. • MARCH 1968

NASA TN D-4441

SIMILARITY SOLUTION FOR TURBULENT MIXING BETWEEN A JET AND A FASTER MOVING COAXIAL STREAM

By Leo F. Donovan

Lewis Research Center
Cleveland, Ohio

NATIONAL AERONAUTICS AND SPACE ADMINISTRATION

For sale by the Clearinghouse for Federal Scientific and Technical Information
Springfield, Virginia 22151 – CFSTI price $3.00

SIMILARITY SOLUTION FOR TURBULENT MIXING BETWEEN A JET AND A FASTER MOVING COAXIAL STREAM

by Leo F. Donovan

Lewis Research Center

SUMMARY

An analysis of turbulent mixing of a jet with a faster moving coaxial stream is presented, and a similarity solution is obtained for large initial ratios of coaxial-stream velocity to jet velocity. The analysis is compared with experimental data, and the velocity profiles at different axial positions are shown to be similar. Centerline velocities follow the predicted behavior reasonably well except for the smallest experimental velocity ratio; half-radii, an indication of the amount of jet spreading, vary as expected after a certain axial distance. The shear-stress distributions are not similar, even at the largest axial positions for which data are available. In addition, the similarity solution is extended to include constant-density mass transfer or heat transfer.

INTRODUCTION

The similarity solution for mixing of a turbulent free jet with a quiescent ambient stream is well known and is discussed in reference 1. For a circular jet, the flow becomes similar beyond an axial position of about 14 jet radii. Velocity profiles are represented by a Gaussian probability function, the centerline velocity decay is inversely proportional to axial distance, and the half-radius, that is, the position at which the local velocity is the average of centerline and coaxial-stream velocities, is proportional to axial distance. When the coaxial stream is moving, it is advantageous to use the difference between the local axial velocity and the coaxial-stream velocity, rather than the local axial velocity alone, as the dependent variable. Radial profiles at a given axial position are then expressed as the ratio of this local difference to the maximum (i. e., centerline) difference at that axial position. It was shown by Forstall and Shapiro (ref. 2) that when a coaxial stream is moving more slowly than the jet, the flow becomes similar after about 8 to 20 radii, depending on the initial ratio of coaxial-stream velocity to jet

velocity. Velocity profiles can be represented by a cosine, 3/2 power, or error curve. Centerline velocity difference was proportional to axial distance, and half-radius was a function of axial position and the initial ratio of jet velocity to coaxial-stream velocity. The wake behind a disk was investigated by Cooper and Lutzky (ref. 3), who found velocity profiles similar beyond 40 radii, centerline velocity difference proportional to the -2/3 power of axial position, and half-radius proportional to the 1/3 power of axial position.

When the coaxial stream is moving faster than the jet, the jet mixing solutions mentioned previously are not applicable. However, in view of the success of these solutions in describing velocity profiles, it seems reasonable to ask whether a similarity solution exists for turbulent mixing of a jet with a faster moving coaxial stream. If such a solution exists, does the real flow exhibit similar velocity profiles, at least in a region of the flow field? If so, it only remains to compare the analysis and data to determine the constants of proportionality that arise in the similarity solution. A similarity solution is obtained for the turbulent mixing of a jet with a faster moving coaxial stream when the initial ratio of coaxial stream velocity to jet velocity is large. The results of the analysis are compared with available experimental data that illustrate similarity behavior in part.

SYMBOLS

C_1, C_2, C_3	proportionality constants
f	dimensionless velocity, $U/U_{\text{¢}}$
g	dimensionless mass fraction, $Y/Y_{\text{¢}}$
h	dimensionless shear stress, $\sigma/\rho U_{\text{¢}}^2$
i	dimensionless mass flux, $\tau/\rho U_{\text{¢}} Y_{\text{¢}}$
K, K_1, K_2, K_3, K_4	constants
k	proportionality constant in eddy viscosity expression
r	radial position
r_j	diameter of jet discharge tube
Sc_t	turbulent Schmidt number
U	coaxial-stream velocity minus local axial velocity
V	radial velocity
W	axial velocity

x axial position

Y coaxial-stream mass fraction minus local mass fraction

ϵ eddy viscosity, $kr_{1/2}U_{\text{¢}}$

η similarity variable, $(r/r_j)\varphi$

ξ dimensionless axial position, x/r_j

ρ density

σ turbulent shear stress, $\rho\epsilon(\partial W/\partial r)$

τ turbulent mass flux, $(\rho\epsilon/Sc_t)(\partial Y/\partial r)$

φ function of axial position

χ dimensionless centerline mass fraction difference, $Y_{\text{¢}}/Y_j$

ψ dimensionless centerline velocity difference, $U_{\text{¢}}/U_j$

Subscripts:

¢ centerline

e coaxial stream

j initial jet

1/2 position at which $U/U_{\text{¢}} = 1/2$

ANALYSIS

Differential Equations and Boundary Conditions

The equations that will be used to describe turbulent jet mixing are the time-averaged continuity equation and the boundary-layer form of the Navier-Stokes equation. Molecular transport will be negligible compared with turbulent transport and can be ignored. The constant-density axisymmetric forms of the equation are (ref. 1)

$$\frac{\partial}{\partial x}(W) + \frac{1}{r}\frac{\partial}{\partial r}(rV) = 0 \tag{1}$$

and

$$\rho W\frac{\partial}{\partial x}(W) + \rho V\frac{\partial}{\partial r}(W) = \frac{1}{r}\frac{\partial}{\partial r}(r\sigma) \tag{2}$$

The initial and boundary conditions for the problem are

$$W = W_j \qquad 0 \le r < r_j \qquad x = 0 \tag{3}$$

$$W = W_e \qquad r > r_j \qquad x = 0 \tag{4}$$

$$\frac{\partial W}{\partial r} = 0, \quad V = 0 \qquad r = 0 \qquad x \ge 0 \tag{5}$$

$$W = W_e \qquad r \to \infty \qquad x \ge 0 \tag{6}$$

A schematic drawing showing the velocities is given in figure 1.

When the coaxial-stream velocity is large compared with the initial jet velocity, the flow will be more wakelike than jetlike. It is shown in reference 3 that, for wake flows, the radial velocity is small far downstream. The approximation that the radial velocity is small is used in the present work to simplify the momentum equation; the results will thus be restricted to regions far enough downstream that the approximation is valid. It will be more convenient to work in terms of a velocity difference

$$U = W_e - W \tag{7}$$

than in terms of a velocity. The momentum equation can be made dimensionless with the initial velocity difference and jet radius and, when V is small, written as

$$\frac{W_e - U}{U_j} \frac{\partial}{\partial\left(\frac{x}{r_j}\right)}\left(\frac{U}{U_j}\right) = -\frac{1}{\frac{r}{r_j}} \frac{\partial}{\partial\left(\frac{r}{r_j}\right)}\left(\frac{r}{r_j} \frac{\sigma}{\rho U_j^2}\right) \tag{8}$$

The boundary conditions are then

$$\frac{\partial}{\partial\left(\frac{r}{r_j}\right)}\left(\frac{U}{U_j}\right) = 0 \qquad \frac{r}{r_j} = 0 \qquad \frac{x}{r_j} \ge 0 \tag{9}$$

$$U = 0 \qquad \frac{r}{r_j} \to \infty \qquad \frac{x}{r_j} \ge 0 \tag{10}$$

Similarity Solution

The flow is expected to be similar after a certain distance. In this region, put

$$\frac{U}{U_{\text{¢}}} = f(\eta) \tag{11}$$

$$\frac{\sigma}{\rho U_{\text{¢}}^2} = h(\eta) \tag{12}$$

$$\frac{U_{\text{¢}}}{U_j} = \psi(\xi) \tag{13}$$

where

$$\eta = \frac{r}{r_j}\,\varphi(\xi) \tag{14}$$

and

$$\xi = \frac{x}{r_j} \tag{15}$$

Roman letters are used for functions of the similarity variable η, and Greek letters are used for functions of the axial variable ξ. The momentum equation then becomes

$$\left(\frac{W_e}{U_j} - f\psi\right)\left(f\frac{d\psi}{d\xi} + \frac{\psi}{\varphi}\frac{d\varphi}{d\xi}\eta\frac{df}{d\eta}\right) = -\varphi\psi^2\frac{1}{\eta}\frac{d}{d\eta}(\eta h) \tag{16}$$

with boundary conditions

$$\frac{df}{d\eta}(0) = 0 \tag{17}$$

$$f(\infty) = 0 \tag{18}$$

For downstream, when the coaxial-stream velocity is large compared with the local velocity difference (i.e., $W_e >> U$), equation (8) can be integrated to yield the integral momentum equation; if $\lim_{r/r_j \to \infty} \left(r/r_j \, \sigma/\rho U_j^2\right) = 0$, then

$$\frac{W_e}{U_j} \frac{\partial}{\partial \xi} \int_0^\infty \frac{U}{U_j} \frac{r}{r_j} d\left(\frac{r}{r_j}\right) = 0 \tag{19}$$

or

$$\int_0^\infty \frac{U}{U_j} \frac{r}{r_j} d\left(\frac{r}{r_j}\right) = K \tag{20}$$

where K is a constant. Equation (20) can be written

$$\frac{\psi}{\varphi^2} \int_0^\infty f\eta \, d\eta = K \tag{21}$$

Since the integral is independent of axial position, it is necessary that

$$\int_0^\infty f\eta \, d\eta = K \frac{\varphi^2}{\psi} = \frac{1}{K_1} \tag{22}$$

where K_1 is a constant. It follows that

$$\frac{d\psi}{d\xi} = 2KK_1 \varphi \frac{d\varphi}{d\xi} \tag{23}$$

so that the momentum equation, when $W_e >> U$, becomes

$$\frac{W_e}{U_j} \frac{d\varphi}{d\xi} \left(2f + \eta \frac{df}{d\eta}\right) = -KK_1 \varphi^4 \frac{1}{\eta} \frac{d}{d\eta} (\eta h) \tag{24}$$

In order for there to be similarity, it is necessary that the terms containing ξ be proportional to the terms containing η in equation (24). Thus,

$$\frac{W_e}{U_j}\frac{d\varphi}{d\xi} = -KK_1K_2\varphi^4 \tag{25}$$

and

$$2f + \eta\frac{df}{d\eta} = \frac{1}{K_2}\frac{1}{\eta}\frac{d}{d\eta}(\eta h) \tag{26}$$

where K_2 is a constant. A solution to equation (25) is

$$\frac{1}{\varphi^3} = 3KK_1K_2\frac{U_j}{W_e}\xi \tag{27}$$

The constant of integration has been dropped since it is small compared with the term retained far downstream. Then, from equation (22),

$$\psi = KK_1\varphi^2 = \left(\frac{3K_2}{K^{1/2}K_1^{1/2}}\frac{U_j}{W_e}\xi\right)^{-2/3} \tag{28}$$

Equation (26) can be written as

$$\frac{d}{d\eta}(\eta^2 f) = \frac{1}{K_2}\frac{d}{d\eta}(\eta h) \tag{29}$$

and integrated using the boundary condition at $\eta = 0$ to give

$$\eta f = \frac{1}{K_2}h \tag{30}$$

The turbulent shear stress can be expressed as

$$\sigma = \rho\epsilon\frac{\partial W}{\partial r} = -\frac{\rho\epsilon}{r_j}U_{\text{¢}}\frac{\partial}{\partial\left(\frac{r}{r_j}\right)}\left(\frac{U}{U_{\text{¢}}}\right) \tag{31}$$

so that

$$h = -\frac{\epsilon}{r_j U_{\text{¢}}} \varphi \frac{df}{d\eta} \tag{32}$$

Thus, equation (30) becomes

$$\frac{df}{d\eta} + \frac{K_2 r_j U_{\text{¢}}}{\epsilon \varphi} \eta f = 0 \tag{33}$$

It is usually assumed in turbulent jet mixing analyses that eddy viscosity is independent of radial position. If Prandtl's postulate that

$$\epsilon = k r_{1/2} U_{\text{¢}} \tag{34}$$

is used, the coefficient in equation (33) becomes

$$\frac{K_2 r_j U_{\text{¢}}}{\epsilon \varphi} = \frac{K_2}{k} \frac{1}{\eta_{1/2}} \tag{35}$$

where $\eta_{1/2} = (r_{1/2}/r_j)\varphi$. Since $\eta_{1/2}$, that is, the value of η at which $f = 0.5$, is constant, equation (33) can be integrated to yield

$$f = \exp\left(-\frac{K_2 r_j}{2k r_{1/2} \varphi} \eta^2\right) \tag{36}$$

Evaluating equation (36) at the half-radius, where $f = 0.5$, gives

$$\ln \frac{1}{2} = -0.693 = -\frac{K_2 r_j}{2k r_{1/2} \varphi} \eta_{1/2}^2 \tag{37}$$

Thus, the velocity profiles are given by

$$f = \exp\left[-0.693\left(\frac{\eta}{\eta_{1/2}}\right)^2\right] = \exp\left[-0.693\left(\frac{r}{r_{1/2}}\right)^2\right] \tag{38}$$

Equation (37) yields

$$\eta_{1/2} = \frac{2(0.693)k}{K_2} \tag{39}$$

or

$$\frac{r_{1/2}}{r_j} = \frac{2(0.693)}{K_2}\,\frac{1}{\varphi} \tag{40}$$

Using equation (22) yields

$$\frac{r_{1/2}}{r_j} = 2(0.693)k\left(\frac{KK_1}{K_2^2}\,\frac{1}{\psi}\right)^{1/2} \tag{41}$$

Equation (22) can be integrated with the help of equation (38) to give

$$\frac{1}{2(0.693)}\,\eta_{1/2}^2 = K\,\frac{\varphi^2}{\psi} \tag{42}$$

and, since $\eta_{1/2} = r_{1/2}/r_j\,\varphi$,

$$\frac{r_{1/2}}{r_j} = \left[2(0.693)K\,\frac{1}{\psi}\right]^{1/2}$$

Equations (41) and (43) can be used to eliminate K_1 and K_2 from equation (28) to give

$$\psi = [2(0.693)]^{-1/3}\left(\frac{3k}{K^{1/2}}\,\frac{U_j}{W_e}\,\xi\right)^{-2/3} \tag{44}$$

Then, equation (43) can be written

$$\frac{r_{1/2}}{r_j} = [2(0.693)]^{2/3}\left(3Kk\,\frac{U_j}{W_e}\,\xi\right)^{1/3} \tag{45}$$

Equations (30), (38), and (39) yield the shear-stress distribution

$$h = 2(0.693)k \frac{r}{r_{1/2}} \exp\left[-0.693\left(\frac{r}{r_{1/2}}\right)^2\right] \tag{46}$$

The limiting case when the initial ratio of coaxial-stream velocity to jet-stream velocity becomes infinite corresponds to wake flow. It is to be noted that the functional forms of the expressions for centerline velocity and half-radius (given by eqs. (44) and (45)) reduce to those found by Cooper and Lutzky (ref. 3) in their wake-flow investigation.

Mass Transfer or Heat Transfer

The analogy between the turbulent transport processes allows the analysis to be extended to account for mass transfer or heat transfer as long as density remains constant. The same procedure is employed to solve the diffusion equation or energy equation as was used to solve the momentum equation; in addition, the solution of the momentum equation is used. The dimensionless diffusion equation can be written in terms of a mass fraction difference analogous to the velocity difference as

$$\frac{W_e - U}{U_j} \frac{\partial}{\partial\left(\frac{x}{r_j}\right)}\left(\frac{Y}{Y_j}\right) = \frac{1}{\frac{r}{r_j}} \frac{\partial}{\partial\left(\frac{r}{r_j}\right)}\left(\frac{r}{r_j} \frac{\tau}{\rho U_j Y_j}\right) \tag{47}$$

with boundary conditions

$$\frac{\partial}{\partial\left(\frac{r}{r_j}\right)}\left(\frac{Y}{Y_j}\right) = 0 \qquad \frac{r}{r_j} = 0 \qquad \frac{x}{r_j} \geq 0 \tag{48}$$

$$Y = 0 \qquad \frac{r}{r_j} \to \infty \qquad \frac{x}{r_j} \geq 0 \tag{49}$$

In the region where the flow is similar put

$$\frac{Y}{Y_{\text{¢}}} = g(\eta) \tag{50}$$

$$\frac{\tau}{\rho U_{\ell} Y_{\ell}} = i(\eta) \tag{51}$$

$$\frac{Y_{\ell}}{Y_j} = \chi(\xi) \tag{52}$$

The definitions of η and ξ are the same as for the solution of the momentum equation, namely,

$$\eta = \frac{r}{r_j} \varphi(\xi) \tag{53}$$

$$\xi = \frac{x}{r_j} \tag{54}$$

The diffusion equation can then be written as

$$\left(\frac{W_e}{U_j} - f\psi\right)\left(g \frac{d\chi}{d\xi} + \frac{\chi}{\varphi} \frac{d\varphi}{d\xi} \eta \frac{d\varphi}{d\eta}\right) = \varphi\chi\psi \frac{1}{\eta} \frac{d}{d\eta} (\eta i) \tag{55}$$

with boundary conditions

$$\frac{dg}{d\eta}(0) = 0 \tag{56}$$

$$g(\infty) = 0 \tag{57}$$

Far downstream, when $W_e >> U$, equation (47) can be integrated to yield

$$\int_0^{\infty} \frac{Y}{Y_j} \frac{r}{r_j} d\left(\frac{r}{r_j}\right) = K_3 \tag{58}$$

where K_3 is a constant. This equation can be written as

$$\frac{\chi}{\varphi^2}\int_0^\infty g\eta\, d\eta = K_3 \tag{59}$$

or

$$\int_0^\infty g\eta\, d\eta = K_3\frac{\varphi^2}{\chi} = \frac{1}{K_4} \tag{60}$$

where K_4 is a constant. Then

$$\frac{d\chi}{d\xi} = 2K_3K_4\varphi\frac{d\varphi}{d\xi} \tag{61}$$

and, when equation (22) is used, equation (55) becomes

$$\frac{W_e}{U_j}\frac{d\varphi}{d\xi}\left(2g + \eta\frac{dg}{d\eta}\right) = KK_1\varphi^4\frac{1}{\eta}\frac{d}{d\eta}(\eta i) \tag{62}$$

In order for there to be similarity, it is again necessary that the terms containing ξ be proportional to the terms containing η. Thus, in light of equation (25),

$$\frac{W_e}{U_j}\frac{d\varphi}{d\xi} = -KK_1K_2\varphi^4 \tag{63}$$

which has already been solved, and

$$2g + \eta\frac{dg}{d\eta} = -\frac{1}{K_2}\frac{1}{\eta}\frac{d}{d\eta}(\eta i) \tag{64}$$

This equation can be written as

$$\frac{d}{d\eta}(\eta^2 g) = -\frac{1}{K_2}\frac{d}{d\eta}(\eta i) \tag{65}$$

Integrating and using the boundary condition at $\eta = 0$ give

$$\eta g = -\frac{1}{K_2} i \tag{66}$$

The turbulent mass flux can be expressed as

$$\tau = \frac{\rho \epsilon}{r_j Sc_t} Y_{\ell} \frac{\partial}{\partial\left(\frac{r}{r_j}\right)}\left(\frac{Y}{Y_{\ell}}\right) \tag{67}$$

where ϵ is given by equation (34). Then

$$i = \frac{\epsilon}{Sc_t r_j} \frac{\varphi}{U_{\ell}} \frac{dg}{d\eta} \tag{68}$$

so that equations (66) and (68) give

$$\frac{dg}{d\eta} + \frac{K_2 Sc_t r_j U_{\ell}}{\epsilon \varphi} \eta g = 0 \tag{69}$$

This equation can be integrated to yield

$$g = \exp\left(-\frac{K_2 Sc_t r_j U_{\ell}}{2\epsilon\varphi} \eta^2\right) \tag{70}$$

Using equation (39) gives

$$g = \exp\left[-0.693\, Sc_t \left(\frac{\eta}{\eta_{1/2}}\right)^2\right] \tag{71}$$

and thus

$$g = f^{Sc_t} \tag{72}$$

The decay of centerline mass fraction can be obtained when equation (60) is integrated and equation (71) is used. Thus, using also equation (22),

$$\chi \sim Sc_t \psi \tag{73}$$

For heat transfer, mass-fraction differences are replaced by temperature differences and the turbulent Schmidt number is replaced by the turbulent Prandtl number.

RESULTS AND DISCUSSION

The functional forms of the variables that describe the turbulent mixing of a jet with a faster moving coaxial stream were determined by the analysis. Experimental data are required to evaluate the proportionality constants that arise; these constants were obtained from an experiment (ref. 4) in which time-averaged velocities and Reynolds stresses were measured with a constant-temperature hot-film anemometer. The duct was large compared with the jet discharge tube in order to minimize the effects of duct walls on the flow. Air was used for both the jet and the coaxial stream. Initial ratios of coaxial-stream velocity to jet velocity varied from 3.4 to 39.5 at a constant Reynolds number (based on coaxial-stream velocity and jet discharge tube diameter) of 2×10^4. Most of the measurements were made within the first 30 jet radii downstream of the jet discharge tube.

Much of this jet mixing data is not far enough downstream to satisfy the restriction imposed in the derivation of the similarity solution, namely, that the coaxial-stream velocity is much larger than the difference between the coaxial-stream velocity and the local velocity. However, inspection of the data in figures 2 to 6 shows that the behavior predicted by the similarity solution is exhibited at smaller axial positions than would be expected. Although the data at the smallest axial positions do no follow this behavior, they are included to illustrate that the similarity solution is not everywhere valid. Also, the data at the lowest initial ratio of coaxial-stream velocity to jet velocity are included to show that the similarity solution is not valid at this low a ratio except possibly at the farthest axial position.

Equations (44) and (45) relate centerline velocity difference and half-radius to relative axial position. The jet mixing data were used to determine the constants in these equations. The data are plotted in figures 2 and 3, and a line with the slope indicated by equation (44) or (45) is drawn through the downstream points. These equations then become

$$\psi = 1.88\left(\frac{U_j}{W_e}\,\xi\right)^{-2/3} \tag{74}$$

$$\frac{r_{1/2}}{r_j} = 0.44\left(\frac{U_j}{W_e}\,\xi\right)^{1/3} \tag{75}$$

The wake-flow data in the downstream region reported (ref. 5) showed that a more rapid decay of centerline velocity difference and, correspondingly, a more rapid spreading of the mixing region had occurred. The difference in behavior may be due to the boundary layer that was present on the jet discharge tube. As a result, the mixing was delayed so that a more narrow mixing region was formed. This is consistent with the observation that the wake centerline velocity difference data, after the mean eddy pocket, decay as the inverse square of axial position before exhibiting the inverse 2/3 power behavior of the similarity solution; however, the centerline velocity difference data from the jet mixing experiments follow the similarity behavior throughout the entire axial region investigated.

The relation given by equation (43) shows that half-radius varies inversely as the square root of centerline velocity difference and is explicitly independent of axial position. Half-radius is plotted as a function of centerline velocity difference in figure 4 and a line with a slope of -1/2 is drawn through the downstream points using the constant K determined from figures 2 and 3. Equation (43) becomes

$$\frac{r_{1/2}}{r_j} = 0.60\,\psi^{-1/2} \tag{76}$$

The downstream data points cluster around the line so determined. The constant is nearly the same as that found in reference 5 for wake flow behind a disk. With k determined, the eddy viscosity expression can be evaluated and equation (34) becomes

$$\epsilon = 0.0056\, r_{1/2} U_{\text{¢}} \tag{77}$$

For comparison with a different physical situation, the proportionality constant for a jet mixing with a quiescent ambient stream is about 0.02 (ref. 1).

The experimental velocity data for five initial velocity ratios are plotted separately in figures 5(a) to (e) along with the line calculated from equation (38); all the data and the line calculated from equation (38) are shown in figure 5(f). The agreement at all velocity ratios is good except at the smallest axial positions. The shear-stress profiles are shown in figure 6. The line calculated from equation (46) by using the value of k determined from figures 2 and 3 is also shown. The profiles are not similar at the largest axial distances and fall below the prediction. Predicted shear-stress distributions for

turbulent jet mixing with a quiescent ambient stream also lie above experimental data (ref. 1).

Data are not available to determine the proportionality constants for the variations of centerline mass fraction or temperature. A reasonable first approximation would be to take the turbulent Schmidt or Prandtl number as 0.7 and use the same proportionality constant as centerline velocity difference variation, that is, 1.88.

CONCLUSIONS

A similarity solution for turbulent mixing of a jet with a faster moving coaxial stream was derived for large initial ratios of coaxial-stream velocity to jet velocity. The solution was compared with data from an experiment in which both the jet and the coaxial stream were air. For initial ratios of coaxial-stream velocity to jet velocity from 3.4 to 39.5 and axial distances from 2.8 to 30 jet radii, the conclusions are as follows:

1. The radial velocity profiles are similar and follow a Gaussian probability function. In terms of a velocity difference $U = W_e - W$,

$$\frac{U}{U_{\text{¢}}} = \exp\left[-0.693\left(\frac{r}{r_{1/2}}\right)^2\right]$$

where W_e is the coaxial-stream velocity, W is the local axial velocity, $U_{\text{¢}}$ is the centerline velocity difference, r is the radial position, and $r_{1/2}$ is the radial position at which $U/U_{\text{¢}} = 1/2$. This even appears to be true upstream of the position where the experimental half-radii vary as the similarity solution predicts.

2. The similarity solution indicates that the centerline velocity can be represented as

$$\frac{U_{\text{¢}}}{U_j} = C_1\left(\frac{U_j}{W_e}\,\frac{x}{r_j}\right)^{2/3}$$

where U_j is the initial jet velocity difference; C_1 is the proportionality constant, equal to 1.88; x is the axial position; and r_j is the diameter of the jet discharge tube. The data follow this behavior reasonably well for the range of axial distances investigated except for the lowest velocity ratio.

3. The half-radius variation predicted by the similarity solution is

$$\frac{r_{1/2}}{r_j} = C_2\left(\frac{U_j}{W_e}\frac{x}{r_j}\right)^{1/3}$$

where C_2 is the proportionality constant, equal to 0.44. The experimental values of half-radius cluster around 0.9 jet radius before following the similarity behavior.

4. The shear-stress profile predicted by the similarity solution is

$$\frac{\sigma}{\rho U_{\text{¢}}^2} = C_3 \frac{r}{r_{1/2}} \exp\left[-0.693\left(\frac{r}{r_{1/2}}\right)^2\right]$$

where σ is the turbulent shear stress; ρ is the density; and C_3 is the proportionality constant, found from the centerline velocity and half-radius variations and equal to 0.078. The experimental shear-stress profiles were not similar, even at the largest axial distances for which data are available.

5. The value of the proportionality constant k in Prandtl's hypothesis for eddy viscosity, $\epsilon = kr_{1/2}U_{\text{¢}}$, was determined to be 0.056. This is about $2\frac{1}{2}$ times the value for jet mixing with a quiescent ambient stream.

6. The analysis was extended to account for constant-density mass transfer or heat transfer between a jet and a coaxial stream. The mass-fraction profiles are

$$\frac{Y}{Y_{\text{¢}}} = \left(\frac{U}{U_{\text{¢}}}\right)^{Sc_t}$$

where Y and $Y_{\text{¢}}$ are the local and centerline values of the coaxial-stream mass fraction minus the local mass fraction, and Sc_t is the turbulent Schmidt number. Centerline mass-fraction variation is given by

$$\frac{Y_{\text{¢}}}{Y_j} \sim Sc_t \frac{U_{\text{¢}}}{U_j}$$

where Y_j is the initial jet mass-fraction difference. For heat transfer, mass-fraction differences are replaced by temperature differences, and the turbulent Schmidt number is

replaced by the turbulent Prandtl number. The experimental data needed to determine the constant of proportionality are not available.

Lewis Research Center,
National Aeronautics and Space Administration,
Cleveland, Ohio, November 9, 1967,
122-28-02-16-22.

REFERENCES

1. Hinze, J. O.: Turbulence. McGraw-Hill Book Co., Inc., 1959.

2. Forstall, Walton, Jr.; and Shapiro, Ascher H.: Momentum and Mass Transfer in Coaxial Gas Jets. J. Appl. Mech., vol. 17, no. 4, Dec. 1950, pp. 399-408.

3. Cooper, Ralph D.; and Lutzky, Morton: Exploratory Investigation of the Turbulent Wakes Behind Bluff Bodies. Rep. No. 963, David Taylor Model Basin, Oct. 1955.

4. Zawacki, Thomas S.: Turbulence in the Mixing Region Between Coaxial Streams. Ph. D. Thesis, Illinois Inst. Tech., 1967.

5. Carmody, Thomas: Establishment of the Wake Behind a Disk. J. Basic Eng., vol. 86, no. 4, Dec. 1964, pp. 869-882.

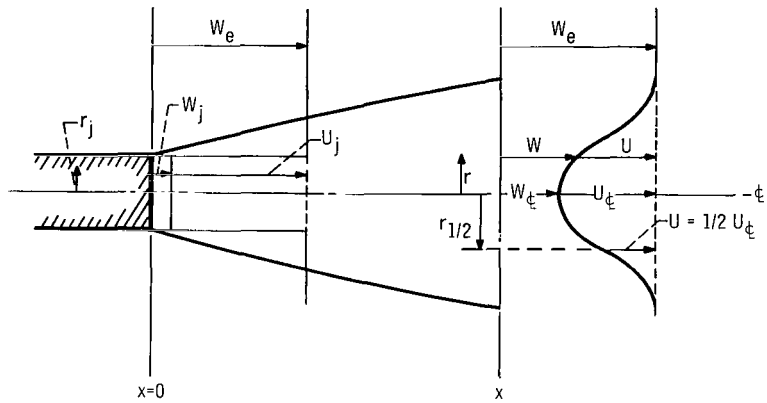

Figure 1. - Schematic diagram of flow field.

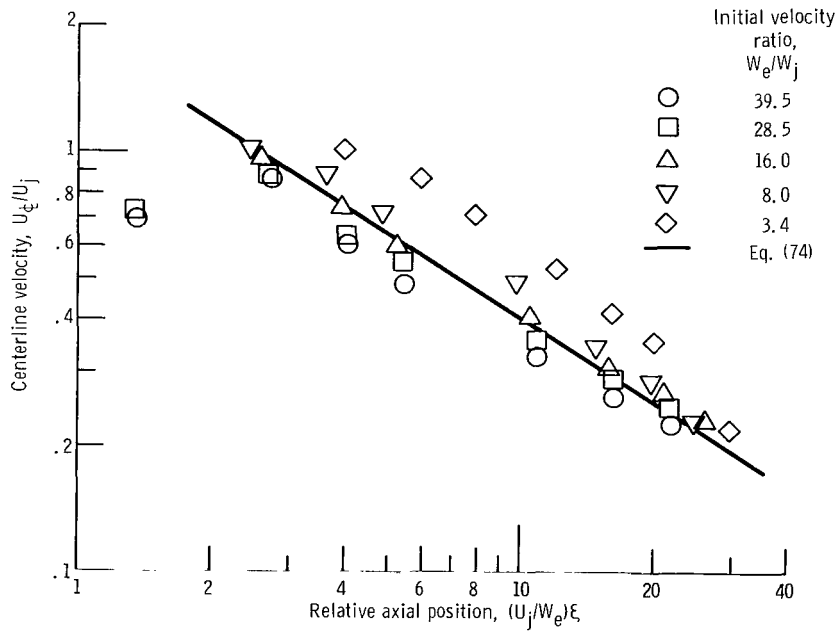

Figure 2. - Axial variation of centerline velocity difference.

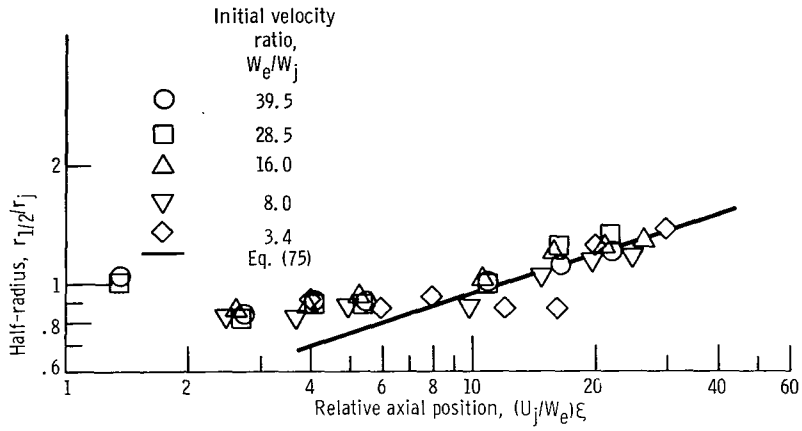

Figure 3. - Axial variation of half-radius.

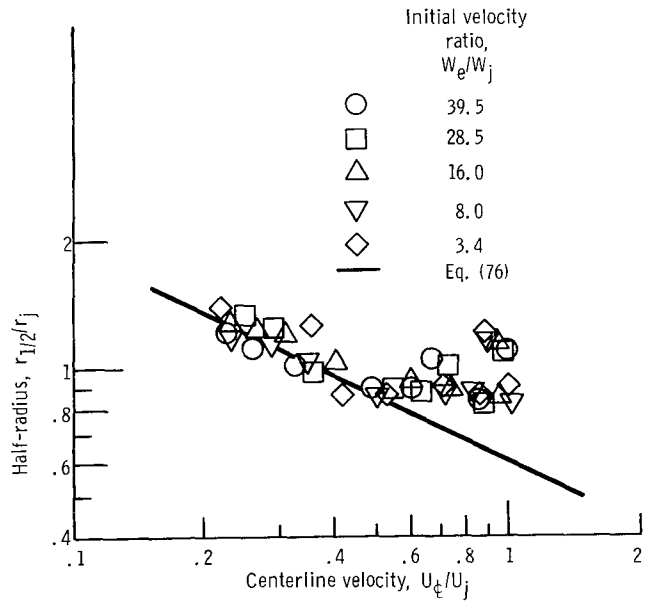

Figure 4. - Relation between half-radius and centerline velocity difference.

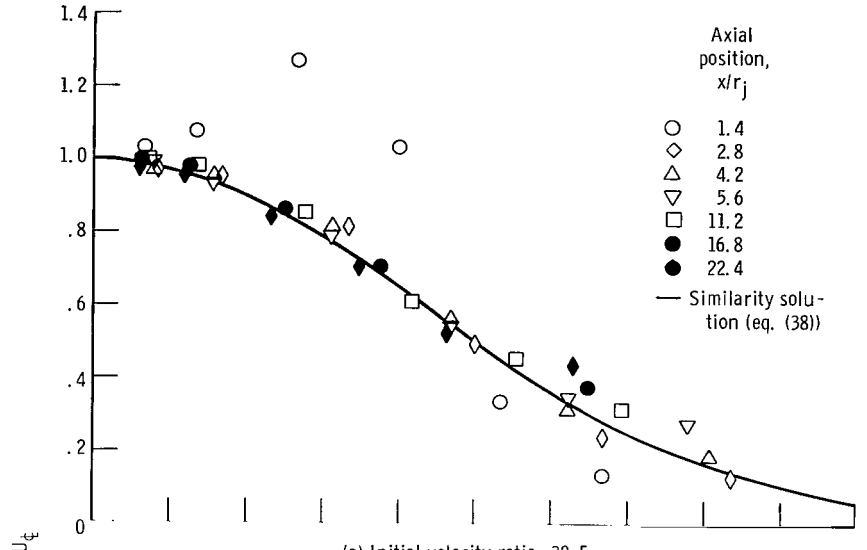

(a) Initial velocity ratio, 39.5.

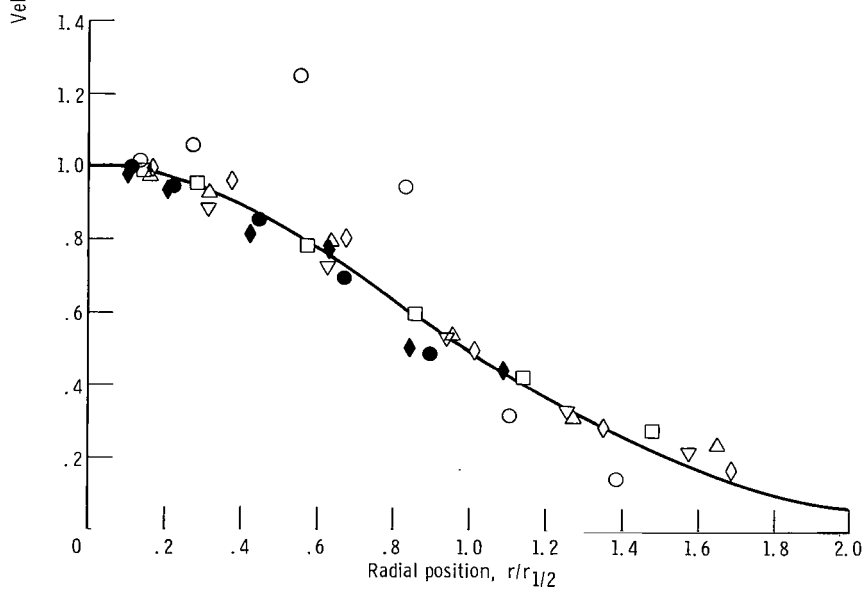

(b) Initial velocity ratio, 28.5.

Figure 5. - Velocity profiles.

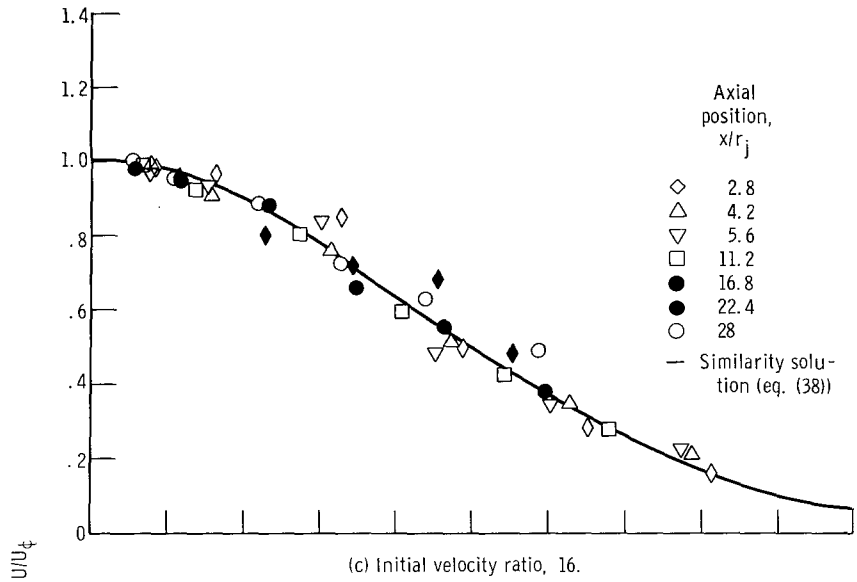

(c) Initial velocity ratio, 16.

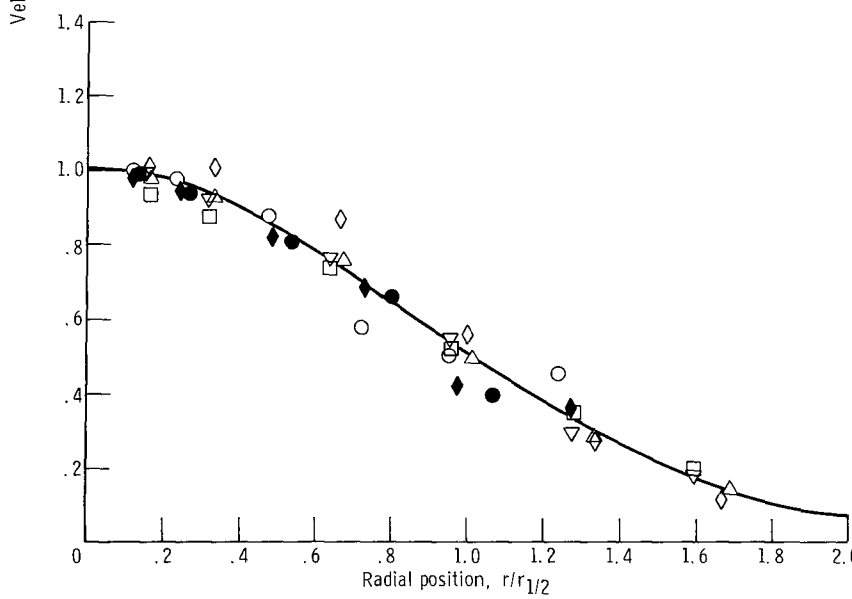

(d) Initial velocity ratio, 8.

Figure 5. - Continued.

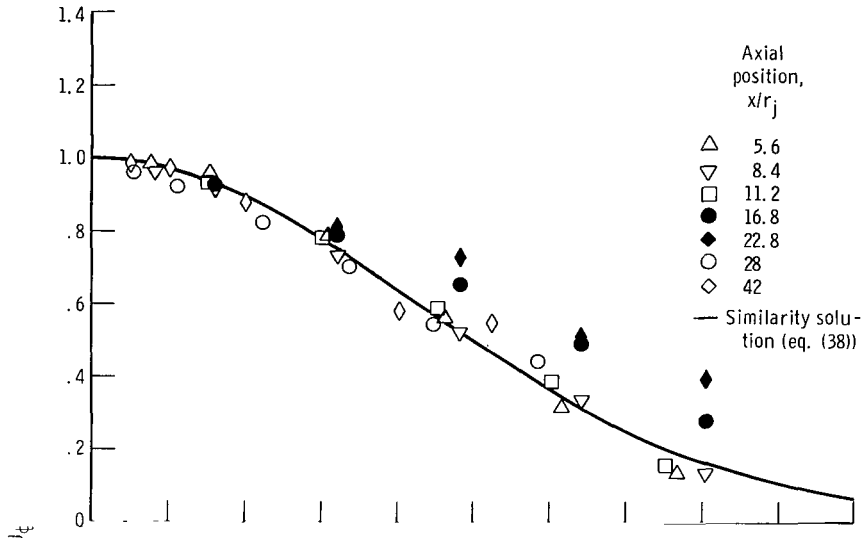

(e) Initial velocity ratio, 3.4.

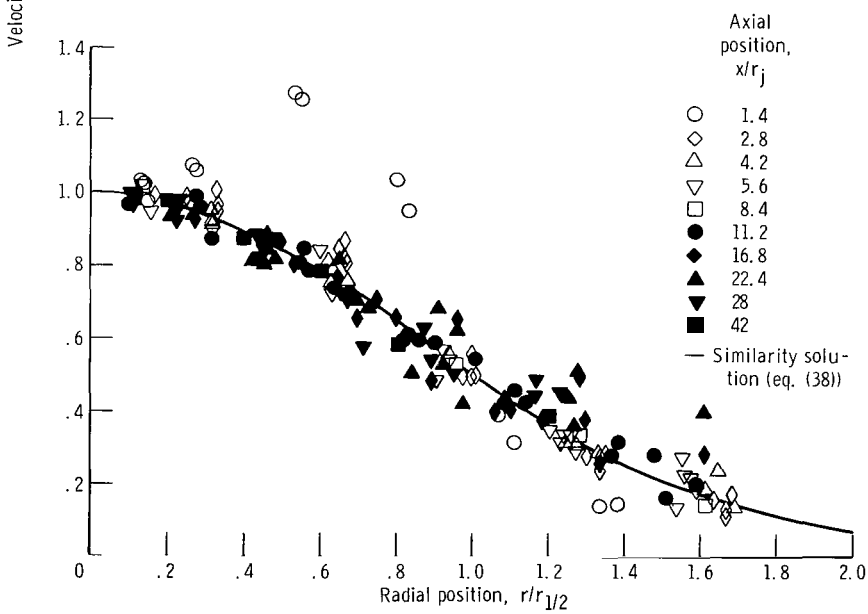

(f) All initial velocity ratios.

Figure 5. - Concluded.

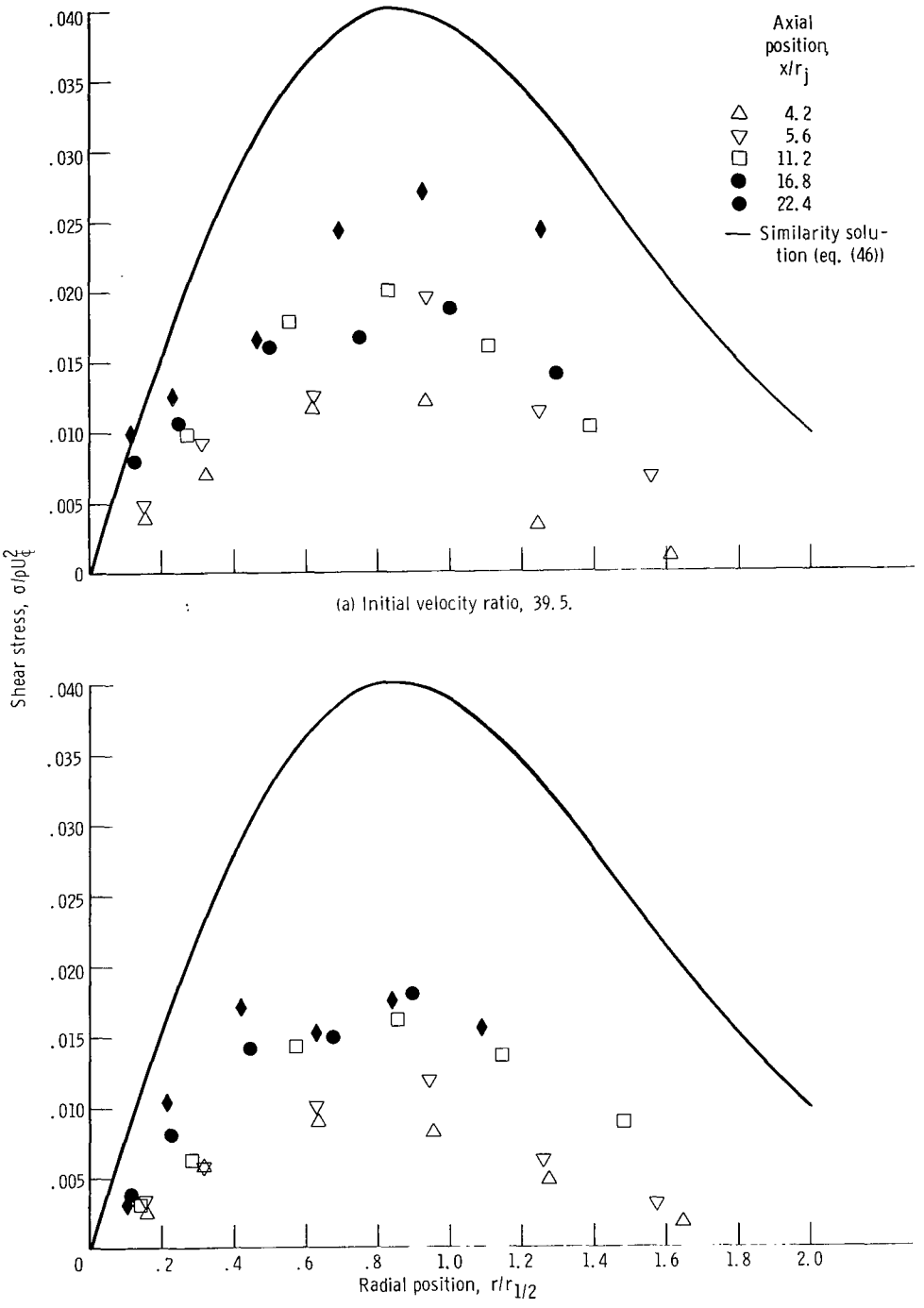

(a) Initial velocity ratio, 39.5.

(b) Initial velocity ratio, 28.5.

Figure 6. - Shear-stress profiles.

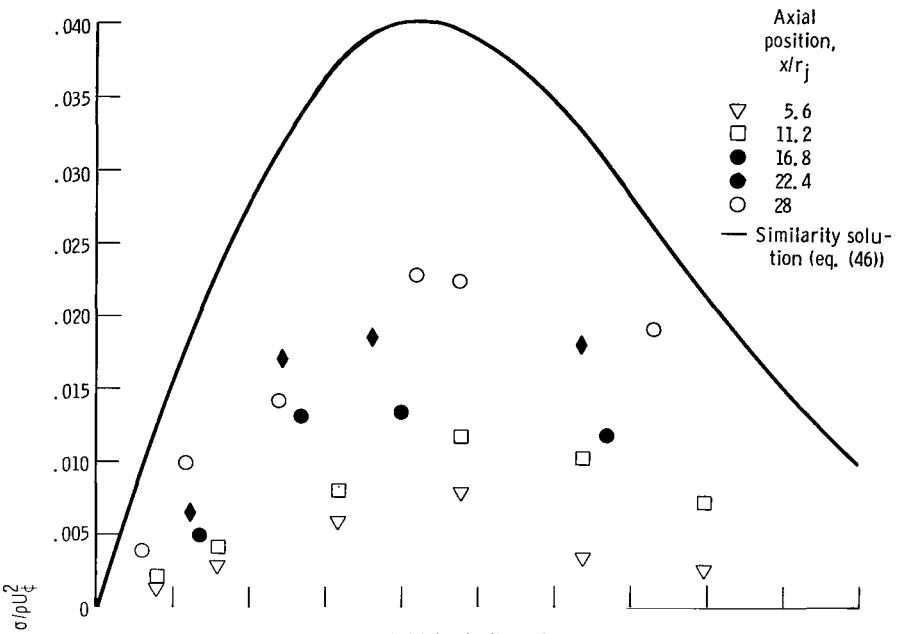

(c) Initial velocity ratio, 8.

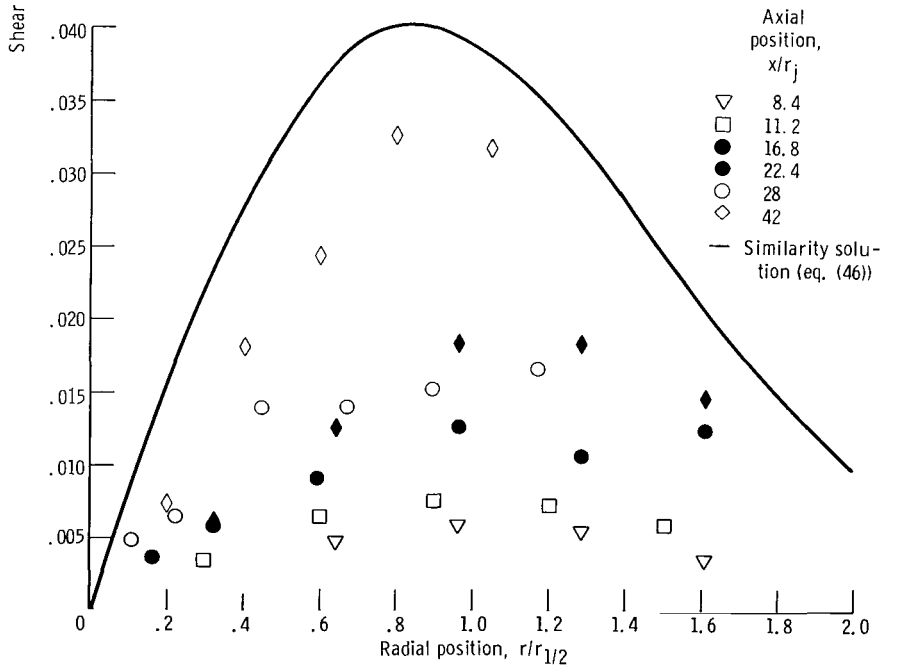

(d) Initial velocity ratio, 3.4.

Figure 6. - Concluded.

"The aeronautical and space activities of the United States shall be conducted so as to contribute . . . to the expansion of human knowledge of phenomena in the atmosphere and space. The Administration shall provide for the widest practicable and appropriate dissemination of information concerning its activities and the results thereof."

—NATIONAL AERONAUTICS AND SPACE ACT OF 1958

NASA SCIENTIFIC AND TECHNICAL PUBLICATIONS

TECHNICAL REPORTS: Scientific and technical information considered important, complete, and a lasting contribution to existing knowledge.

TECHNICAL NOTES: Information less broad in scope but nevertheless of importance as a contribution to existing knowledge.

TECHNICAL MEMORANDUMS: Information receiving limited distribution because of preliminary data, security classification, or other reasons.

CONTRACTOR REPORTS: Scientific and technical information generated under a NASA contract or grant and considered an important contribution to existing knowledge.

TECHNICAL TRANSLATIONS: Information published in a foreign language considered to merit NASA distribution in English.

SPECIAL PUBLICATIONS: Information derived from or of value to NASA activities. Publications include conference proceedings, monographs, data compilations, handbooks, sourcebooks, and special bibliographies.

TECHNOLOGY UTILIZATION PUBLICATIONS: Information on technology used by NASA that may be of particular interest in commercial and other non-aerospace applications. Publications include Tech Briefs, Technology Utilization Reports and Notes, and Technology Surveys.

Details on the availability of these publications may be obtained from:

SCIENTIFIC AND TECHNICAL INFORMATION DIVISION

NATIONAL AERONAUTICS AND SPACE ADMINISTRATION

Washington, D.C. 20546